Cusp-core transformations in dwarf galaxies: observational predictions

Teyssier, R ; Pontzen, A ; Dubois, Y ; Read, J I

Abstract: The presence of a dark matter core in the central kiloparsec of many dwarf galaxies has been a long-standing problem in galaxy formation theories based on the standard cold dark matter paradigm. Recent simulations, based on smooth particle hydrodynamics and rather strong feedback recipes, have shown that it was indeed possible to form extended dark matter cores using baryonic processes related to a more realistic treatment of the interstellar medium. Using adaptive mesh refinement, together with a new, stronger supernova feedback scheme that we have recently implemented in the RAMSES code, we show that it is also possible to form a prominent dark matter core within the well-controlled framework of an isolated, initially cuspy, 1010 M dark matter halo. Although our numerical experiment is idealized, it allows a clean and unambiguous identification of the dark matter core formation process. Our dark matter inner profile is well fitted by a pseudo-isothermal profile with a core radius of 800 pc. The core formation mechanism is consistent with the one proposed by Pontzen Governato. We highlight two key observational predictions of all simulations that find cusp-core transformations: (i) a bursty star formation history with a peak-to-trough ratio of 5 to 10 and a duty cycle comparable to the local dynamical time and (ii) a stellar distribution that is hot with v/ ˜ 1. We compare the observational properties of our model galaxy with recent measurements of the isolated dwarf Wolf-Lundmark-Mellote (WLM). We show that the spatial and kinematical distribution of stars and H I gas are in striking agreement with observations, supporting the fundamental role played by stellar feedback in shaping both the stellar and dark matter distribution.

DOI: https://doi.org/10.1093/mnras/sts563

Monthly Notices
of the
ROYAL ASTRONOMICAL SOCIETY

MNRAS **429,** 3068–3078 (2013) doi:10.1093/mnras/sts563

Cusp-core transformations in dwarf galaxies: observational predictions

Romain Teyssier,[1,2]⋆ Andrew Pontzen,[3] Yohan Dubois[4] and Justin I. Read[5,6]

[1]*Institute for Theoretical Physics, University of Zurich, CH-8057 Zürich, Switzerland*
[2]*CEA Saclay, DSM/IRFU/SAP, Bâtiment 709, F-91191 Gif-sur-Yvette Cedex, France*
[3]*Astrophysics, University of Oxford, Denys Wilkinson Building, Keble Road, Oxford OX1 3RH*
[4]*Institut d'Astrophysique de Paris, 98bis boulevard Arago, F-75014 Paris, France*
[5]*Department of Physics and Astronomy, University of Leicester, University Road, Leicester LE1 7RH*
[6]*Institute for Astronomy, Department of Physics, ETH Zürich, Wolfgang-Pauli-Strasse 27, CH-8093 Zürich, Switzerland*

Accepted 2012 December 5. Received 2012 October 15; in original form 2012 June 5

ABSTRACT

The presence of a dark matter core in the central kiloparsec of many dwarf galaxies has been a long-standing problem in galaxy formation theories based on the standard cold dark matter paradigm. Recent simulations, based on smooth particle hydrodynamics and rather strong feedback recipes, have shown that it was indeed possible to form extended dark matter cores using baryonic processes related to a more realistic treatment of the interstellar medium. Using adaptive mesh refinement, together with a new, stronger supernova feedback scheme that we have recently implemented in the RAMSES code, we show that it is also possible to form a prominent dark matter core within the well-controlled framework of an isolated, initially cuspy, $10^{10}\,\mathrm{M}_{\odot}$ dark matter halo. Although our numerical experiment is idealized, it allows a clean and unambiguous identification of the dark matter core formation process. Our dark matter inner profile is well fitted by a pseudo-isothermal profile with a core radius of 800 pc. The core formation mechanism is consistent with the one proposed by Pontzen & Governato. We highlight two key observational predictions of all simulations that find cusp-core transformations: (i) a bursty star formation history with a peak-to-trough ratio of 5 to 10 and a duty cycle comparable to the local dynamical time and (ii) a stellar distribution that is hot with $v/\sigma \sim 1$. We compare the observational properties of our model galaxy with recent measurements of the isolated dwarf Wolf-Lundmark-Mellote (WLM). We show that the spatial and kinematical distribution of stars and H I gas are in striking agreement with observations, supporting the fundamental role played by stellar feedback in shaping both the stellar and dark matter distribution.

Key words: galaxies: dwarf – ISM: structure – methods: numerical – dark matter.

1 INTRODUCTION

Dwarf galaxies, although very numerous and common in our present day Universe, are also very faint and difficult to observe. Nevertheless, it is now established that star formation proceeds at a very inefficient rate in dwarf galaxies, making them ideal laboratories to study the spatial distribution of their parent dark matter halo. Indeed, if dwarf galaxies are dark matter dominated, a stellar kinematic analysis gives direct constraints on the dark matter mass distribution. Although theoretical predictions of pure *N*-body models favour the formation of a cusp in the inner region of dark matter haloes (Moore 1994; Navarro, Frenk & White 1997), the observed rotation curve of dwarf and low surface brightness galaxies was shown to be more consistent with a shallower profile, even a constant density core (de Blok & McGaugh 1997; de Blok et al. 2001; de Blok & Bosma 2002; Kuzio de Naray, McGaugh & de Blok 2008). This apparent disagreement led to the so-called 'cusp-core' problem, a serious challenge for the currently favoured Cold Dark Matter (CDM) paradigm (Flores & Primack 1994; Moore 1994). Many solutions to this problem have been proposed in the recent years – for example a warm dark matter particle (Kuzio de Naray et al. 2010; Villaescusa-Navarro & Dalal 2011; Macciò et al. 2012) or self-interacting dark matter (Spergel & Steinhardt 2000; Rocha et al. 2012) – but the only explanation consistent with CDM relies on the effect of baryonic physics, and more precisely on stellar feedback, to modify substantially the dark matter distribution.

Mashchenko, Wadsley & Couchman (2008) were the first to find a cusp-core transformation effect in a cosmological simulation, modelling a dwarf galaxy of mass $\sim 10^{9}\,\mathrm{M}_{\odot}$ down to redshift $z \sim 5$.

⋆E-mail: Romain.Teyssier@cea.fr

This has been seen again in a more recent work at higher masses and reaching lower redshifts (Governato et al. 2010; Macciò et al. 2012; Martizzi et al. 2012). A long history of work has looked at the possibility of baryonic physics generating such a transformation: for instance, Navarro, Eke & Frenk (1996) showed that impulsive mass-loss leads to irreversible expansion of orbits near the centre, Read & Gilmore (2005) suggested that repeated epochs of outflows could produce a strong enough effect to generate cores and Mashchenko, Couchman & Wadsley (2006) pointed out that internal bulk motions of gas (not necessarily outflows) could have the same effect. Finally, Pontzen & Governato (2012) (hereafter PG12) produced an analytic model of impulsive heating which was able to make quantitative predictions for the rate of cusp flattening, agreeing with the simulated results of Governato et al. (2010). This demonstrated that impulsive gas motions were the dominant cause of the simulated cusp-core transformations as opposed to, for example, heating due to dynamical friction (e.g. El-Zant, Shlosman & Hoffman 2001; Goerdt et al. 2010).

Although cosmological simulations provide realistic environments and mass accretion histories for the model galaxies, they are often challenging to analyse because of their geometrical and evolutionary complexity. Moreover, since they are time consuming, the force resolution is currently limited to ∼80 pc, which is only one tenth of the measured core radius (Governato et al. 2010). It is therefore quite important to perform additional simulations with both a simpler set-up and a higher resolution, which is precisely the goal of our paper. In Mashchenko et al. (2006), a similar approach was proposed with an isolated Navarro-Frenk-White (NFW) halo stirred by three arbitrarily moving gas clumps. Although the proposed set-up was quite simplistic, it provided a well-controlled experiment of cusp-to-core evolution with a better force resolution of 40 pc. Very recently, Cloet-Osselaer et al. (2012) have performed a series of isolated NFW halo simulations with a more realistic treatment of star formation, stellar feedback and the induced gas motions based on the smoothed particle hydrodynamics (SPH) technique. This work, following up on a series of papers reproducing many properties of the gas and stellar distribution in dwarf galaxies (Valcke, De Rijcke & Dejonghe 2008; Schroyen et al. 2011), also confirmed the formation of a dark matter core.

In this paper, we will also perform idealized simulations of an isolated NFW halo, with a more realistic treatment of the interstellar medium (ISM) physics, and, for the first time, with the Adaptive Mesh Refinement (AMR) code RAMSES (Teyssier 2002). It is indeed important to verify that core formation can also be recovered using a different type of code than the one used so far in all the previously cited papers, namely SPH in two different implementations, GADGET by Springel (2005) and GASOLINE by Wadsley, Stadel & Quinn (2004). As shown by Agertz et al. (2007) and Wadsley, Veeravalli & Couchman (2008), both code types suffer from different systematic effects that might affect the numerical solution, especially when trying to resolve the clumpy ISM (see also Read, Hayfield & Agertz 2010; Read & Hayfield 2012).

The paper is organized as follows: in the first section, we describe the set-up of our numerical experiment, with three different simulations that we would like to compare. We then present and discuss our new stellar feedback implementation in the RAMSES code, which allows us to have a much stronger dynamical effect on the surrounding gas than we were previously able to achieve, without invoking extra sources of energy. In the third section, we present our results, with emphasis put on the dark matter distribution and how the formation of the core correlates with strong potential fluctuations triggered by powerful gas expulsion phases. Finally, we discuss and interpret our results in the light of the recently proposed mechanism by PG12, and confront our findings with observations.

2 SIMULATION SET-UP

We consider an isolated halo in hydrostatic equilibrium with $f_{\rm gas} = 15$ per cent. Both gas and dark matter follows the same NFW density profile, with concentration parameter $c = 10$. The halo circular velocity is chosen to be $V_{200} = 35\ {\rm km\,s^{-1}}$, corresponding to the virial radius $R_{200} = 50\,{\rm kpc}$ (or $35\,{\rm kpc}\,h^{-1}$) and the virial mass $M_{200} = 1.4 \times 10^{10}\,{\rm M}_\odot$ (or $10^{10}\,{\rm M}_\odot\,h^{-1}$). The halo is truncated at 112.5 kpc, so that the total enclosed mass is $M_{\rm tot} = 2 \times 10^{10}\,{\rm M}_\odot$. Following now rather standard prescriptions, such as in Kaufmann et al. (2007) and Dubois & Teyssier (2008), we initialized the gas temperature by solving the hydrostatic equilibrium equation (see equation 1 in Kaufmann et al. 2007, for example), and we set the gaseous halo in slow rotation around the z-axis, using the average angular momentum profile computed from cosmological simulation (Bullock et al. 2001) and a spin parameter $\lambda = 0.04$. For more details on the set-up, the reader can refer to Dubois & Teyssier (2008). We use one million dark matter particles to sample the phase space of our dark matter halo. Initial positions and velocities were computed using the density–potential pair approach of Kazantzidis, Magorrian & Moore (2004), later refined by Read et al. (2006a). To test the stability of our gas dark matter equilibrium system, we ran a first simulation with only adiabatic gas dynamics, without cooling and star formation. As can be seen in Fig. 1, our dark matter halo is stable during 2 Gyr of evolution and does not deviate by more than 10 per cent from the initial NFW distribution, except within 60 pc from the centre (corresponding roughly to twice the cell size), where the deviation can be as high as a factor of 2.

All the simulations presented here have been run using the RAMSES code (Teyssier 2002; Fromang, Hennebelle & Teyssier 2006; Teyssier, Fromang & Dormy 2006). We used a quasi-Lagrangian refinement strategy to build the initial AMR grid, as well as refining and de-refining cells during the course of the simulation; each cell is individually refined if it contains more than eight dark matter particles or if it contains a baryonic mass (gas mass + star particle mass) larger than $8 \times m_{\rm res}$, where $m_{\rm res} = 1500\,{\rm M}_\odot$. Note that our

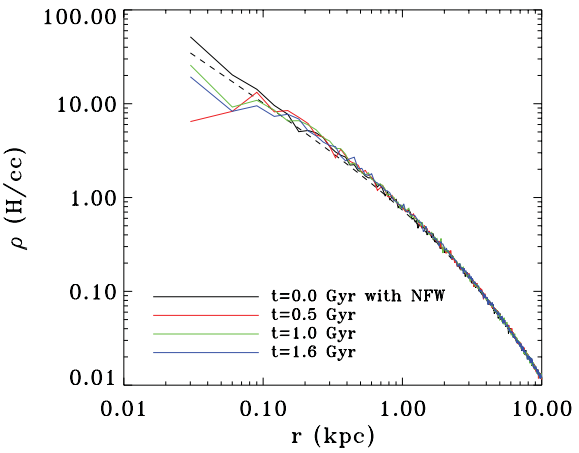

Figure 1. Evolution of the dark matter density profile over the 2 Gyr of evolution for the control run with adiabatic (no cooling and no star formation) hydrodynamics. We see that the dark matter halo density profile remains stable (with at most 10 per cent deviations), except within the central 60 pc, which corresponds to twice the cell size in this case, in which we see less than a factor of 2 deviations from the initial profile.

gas mass resolution corresponds initially to 2 million gas resolution elements across the whole gaseous halo. The box size being set to $L = 300$ kpc (in our terminology this corresponds to the first AMR level $\ell = 1$), we used isolated boundary conditions for the Poisson solver and zero-gradient boundary conditions for the hydro solver. For the latter, we used the HLLC Riemann solver and the MinMod slope limiter (see Fromang et al. 2006 for related details).

Without cooling and star formation, we do not need to specify a maximum level of resolution; we just let the code refine the grid until it runs out of mass in the smallest AMR cell. In our adiabatic simulation, we have indeed reached 'only' level $\ell = 13$ at the very centre of the halo, corresponding to a cell size $\Delta x = 36$ pc. If cooling and star formation are activated, gas dynamics becomes strongly dissipative and nothing can prevent the collapse. It is therefore crucial to set a maximum level of refinement, or a minimum grid resolution. In this paper, we use $\ell_{\rm max} = 14$ or $\Delta x = 18$ pc, which is only a factor of 2 better than in the dark matter only case, therefore avoiding two-body relaxation in the dark matter component. Our limited spatial resolution requires a careful treatment of our thermal model, in order to avoid numerical difficulties. As is now customary in galaxy and star formation simulations, we use an artificial pressure floor designed to enforce that the effective Jeans length is equal to four computational cells (Truelove et al. 1997). This extra-pressure, equal to $P_J \simeq 16G\Delta x^2\rho^2$, is added to the thermal pressure in the Euler equation, gas cooling being applied only to the thermal internal energy. We use standard H and He cooling (Katz, Weinberg & Hernquist 1996), with an additional contribution from metals based on the Sutherland & Dopita (1993) model above 10^4 K and metal fine-structure cooling below 10^4 K as in Rosen & Bregman (1995). Metallicity is modelled as a unique, passively advected quantity, denoted as Z, representing the mass fraction of metals, and seeded by individual supernova event with a yield $y = 0.1$. The initial metallicity in the halo is set to $Z = 10^{-3}\,{\rm Z}_\odot$, enabling from the start cooling down to very low temperatures. With these ingredients and for our spatial resolution of 18 pc, gas will cool efficiently down to $T_J \simeq 600$ K and reach a density of $n_J \simeq 60\,{\rm H\,cm^{-3}}$, before hitting the Jeans-length-related pressure floor (the index J standing for Jeans-length-related quantities). This is a conservative estimate of the maximum gas density we can reach before being affected by finite resolution effects.

Star formation (SF) is modelled using a Schmidt law (Schmidt 1959), for which the SF rate is given by

$$\dot{\rho}_* = \epsilon_* \frac{\rho_{\rm gas}}{t_{\rm ff}} \quad \text{if} \quad \rho_{\rm gas} > \rho_*. \tag{1}$$

The SF efficiency per free-fall time $t_{\rm ff}$ is usually chosen close to a few per cent (Krumholz & Tan 2007); we used here $\epsilon_* = 0.01$. The density threshold for SF, above which gas is considered to be dense enough to be eligible to form stars, has to be chosen carefully. In order to mimic as closely as possible realistic SF in dense molecular clouds, we want to choose this threshold as high as possible. On the other hand, as discussed previously, the gas density distribution in the simulation will be affected by the finite resolution effect close to the Jeans density, in our case $n_J \simeq 60\,{\rm H\,cm^{-3}}$. It is therefore quite natural to choose the SF threshold density close to the Jeans density. In this paper, we conservatively picked $n_* = n_J/3 = 20\ {\rm H\,cm^{-3}}$. These recipes have all been implemented in the RAMSES code and used for many galaxy formation studies in the recent years (Agertz, Teyssier & Moore 2009; Teyssier, Chapon & Bournaud 2010; Bournaud et al. 2011; Agertz, Teyssier & Moore 2011; Scannapieco et al. 2012). We will now present in more detail the main ingredient of this study, namely our new implementation of stellar feedback.

3 STELLAR FEEDBACK IMPLEMENTATION

The last but probably most important ingredient in galaxy formation simulations is stellar feedback. Stars, especially young stars, interact quite strongly with their environment. Among many possible physical processes, H II regions, stellar winds, Type II and Type Ia supernova explosions have been the most popular. These various mechanisms are believed to be responsible for SF regulation in dwarf galaxies (Dekel & Silk 1986), and they contribute collectively to roughly a couple of 10^{51} erg of energy injection into the surrounding ISM, for an average $10\,{\rm M}_\odot$ massive star and for a standard stellar initial mass function (IMF) (Piontek & Steinmetz 2011). Since all these processes occur at very small, sub-pc scales, we have to rely on rather approximate numerical implementations. The simplest approach is clearly to inject directly thermal energy into each gas cell containing young stars. It turns out that feedback is very inefficient in that case because it occurs mostly in dense gas where cooling immediately radiates away the added thermal energy. It is usually considered that this strong cooling is a spurious numerical effect (Ceverino & Klypin 2009). But supernova explosions, and more generally feedback from young stars, takes place in a very dense environment (such as molecular clouds) so that strong radiative effects are likely to take place anyway. More recently, radiative pressure from young stars has also been proposed as a new possible mechanism (Murray, Quataert & Thompson 2010) to drive momentum into the ISM. This approach is very promising since gas momentum does not suffer directly from gas cooling. It is however quite difficult to model since it requires detailed radiative transfer calculation of the infrared radiation reprocessed by dust. It was also shown recently that, for dwarf galaxies such as the ones studied here, supernova feedback likely dominates other sources of feedback energy (Hopkins, Quataert & Murray 2012); radiative effects become inefficient due to the lower column densities.

Physical processes associated with stellar feedback are probably even more complex than the ones quoted here so far. For example, we know from X-ray observations of supernova remnants that they are strongly magnetized and turbulent. Moreover, cosmic rays acceleration occurs very rapidly and the energy density stored in the relativistic component is large enough to affect significantly the dynamics of the propagating shock wave (Ellison, Decourchelle & Ballet 2004; Ferrand et al. 2010). These non-thermal processes have much longer dissipation time-scales than the thermal component, so they can store feedback energy longer than the rapidly cooling gas and release it to the gaseous component more gradually. Modelling unresolved turbulence, magnetic field amplification and cosmic ray propagation and radiative losses in the framework of galaxy formation is at its infancy, although some recent progresses have been reported (Hanasz et al. 2006; Jubelgas et al. 2008; Scannapieco & Brüggen 2010; Uhlig et al. 2012). We propose here a much simpler formalism that captures very crudely these various non-thermal processes and couple more efficiently the energy associated with stellar feedback to the gas component.

The idea is to introduce a new variable for the energy density in these non-thermal components. We note this new variable $e_{\rm turb}$ for simplicity, although it does not have to be associated with turbulence only, but also with cosmic rays and magnetic fields. The specific turbulent energy $\epsilon_{\rm turb}$ is defined by $e_{\rm turb} = \rho\epsilon_{\rm turb}$. We model the time

evolution of this non-thermal energy using the following simple equation:

$$\rho \frac{\mathrm{D}\epsilon_{\rm turb}}{\mathrm{D}t} = \dot{E}_{\rm inj} - \frac{\rho\epsilon_{\rm turb}}{t_{\rm diss}}, \quad (2)$$

where we have only two terms, the non-thermal energy source $\dot{E}_{\rm inj}$ due to stellar feedback and the energy dissipation modelled classically as a damping term with dissipation time-scale $t_{\rm diss}$. The time-scale depends on the exact underlying dissipation mechanism, such as radiative losses for cosmic rays (Enßlin et al. 2007) or eddy turn-over time for turbulence. In what follows, we just need to accumulate enough feedback energy to drive strong outflows and to regulate our SF efficiency across the galactic disc. In this paper, we used a fixed dissipation time-scale

$$t_{\rm diss} \simeq 10\,{\rm Myr} \quad (3)$$

comparable to the typical molecular cloud lifetime, as expected from their observed internal SF efficiency (Williams & McKee 1997). Other options are possible, such as, for example, $t_{\rm diss} \simeq \lambda_{\rm J}/\sigma_{\rm turb}$, where $\lambda_{\rm J}$ could be the typical Jeans length or, equivalently, the typical cell size, or even more exotic, the cosmic rays mean free path or magnetic dissipation length scale. The turbulence velocity dispersion $\sigma_{\rm turb}$ is defined here as

$$\epsilon_{\rm turb} = \frac{1}{2}\sigma_{\rm turb}^2. \quad (4)$$

We parametrized the non-thermal energy injection as

$$\dot{E}_{\rm inj} = \dot{\rho}_* \eta_{\rm SN} 10^{50}\,{\rm erg/M_\odot}, \quad (5)$$

which corresponds to a maximally efficient model for which 10^{51} erg per 10 $\mathrm{M}_\odot$ massive star is injected into non-thermal energy. For a typical IMF, the mass fraction of stars going supernovae is roughly $\eta_{\rm SN} = 0.1$. Although these numbers are determined by stellar evolution models, we believe that they can be considered as free parameters. Indeed, both the IMF and stellar evolution models are poorly constrained at low metallicity and/or at high redshift, and more generally in extreme galactic environments (Marks et al. 2012). Note that this energy is injected in the gas cell only 10 Myr after the star particle has been created.

The final step of our feedback model is to compute the non-thermal pressure using $P_{\rm turb} = \rho\sigma_{\rm turb}^2$ and add it to the thermal pressure to get

$$P_{\rm tot} = P_{\rm thermal} + P_{\rm turb}. \quad (6)$$

This obviously requires to modify the Euler equation by adding the non-thermal pressure term, and this could impact more or less deeply the hydrodynamics solver. One even simpler alternative is to actually add directly to the thermal energy the injected non-thermal energy as

$$\rho \frac{\mathrm{D}\epsilon_{\rm thermal}}{\mathrm{D}t} = \dot{E}_{\rm inj} - P_{\rm thermal}\nabla\cdot\boldsymbol{v} - n_H^2\Lambda \quad (7)$$

and shut down gas cooling to mimic the contribution of the non-thermal pressure to the total pressure. $\epsilon_{\rm turb}$ becomes a completely independent variable (like a passive Lagrangian tracer) used only to re-activate cooling when the non-thermal contribution becomes comparable to or smaller than the thermal energy. In practice, we shut down cooling everywhere the turbulence velocity dispersion is large enough, using

$$\Lambda = 0 \text{ if } \sigma_{\rm turb} > 10\,{\rm km\,s^{-1}}. \quad (8)$$

Our final model does not require any modification to the hydro solver. It just requires to shut down cooling in each cell, if the velocity dispersion is above a chosen threshold (here 10 $\mathrm{km\,s^{-1}}$). The other advantage is that it is qualitatively very similar to the 'delayed cooling' approach used in other recent studies (Stinson et al. 2006; Governato et al. 2010; Agertz et al. 2011), although our current approach is motivated by non-thermal astrophysical processes for which a detailed modelling would be far beyond the scope of this study.

4 EVOLUTION OF THE DARK MATTER DENSITY PROFILE

Now that we have presented our numerical set-up and parameters, we now describe in more details our results. We have performed three different simulations, in order to highlight the effect of stellar feedback on the mass distribution within the halo. The first simulation, already presented in the previous sections, was a pure adiabatic gas evolution of our initial hydrostatic equilibrium halo. We checked that our initial set-up was indeed stable over 2 Gyr time, as it should be since no gas cooling was considered in this case (see Fig. 1). We would like to stress that this is a very important step in our methodology, since it demonstrates that any evolution in the dark matter density profile has to be related to the dissipative nature of baryons, through gas cooling, star formation or feedback. The second simulation was run with (metal dependent) gas cooling and star formation. No stellar feedback was included. In this case, the gas loses pressure support and rains down towards the centre of the halo, quickly reaching the centrifugal barrier and sets up into a centrifugally supported disc. As one can see in Fig. 2, the final disc is very thin and fragments into dense gas clumps that form stars actively. This gives rise to the formation of dense bound star clusters that survive for long times. We also see the formation of a massive bulge in the centre of the galaxy, leading to an overall highly concentrated baryons distribution. The associated SF history can be seen in Fig. 3: it is on average very high, around 1 $\mathrm{M}_\odot\ \mathrm{yr}^{-1}$, with short bursts reaching 4 to 6 $\mathrm{M}_\odot\ \mathrm{yr}^{-1}$, associated with the formation of dense gas clumps. Such a high SF rate is usually associated with massive galaxies at low redshift. This is quite unrealistic for dwarf galaxies we see today (Hopkins, Schulte-Ladbeck & Drozdovsky 2002). The effect of this strongly dissipative evolution on the dark matter profile can be seen in Fig. 4. After 1 Gyr, the dark matter distribution has been adiabatically contracted very significantly by baryons. The inner slope of the dark matter density profile is close to -2, and no core is visible. It is worth mentioning that although we have a very clumpy structure in the ISM and in the stellar distribution, it does not trigger the formation of a dark matter core in our case; the mechanism proposed by Mashchenko et al. (2006) (see also El-Zant et al. 2001) does not work here, probably because our clumps are not massive enough.

We now move to our final run with gas cooling, SF and stellar feedback. The evolution of the star-forming disc is dramatically different from the 'no feedback' run. We see in Fig. 2 that the final gas distribution shows a very thick, turbulent disc, with strong outflows made of shredded clouds and filaments. The face-on view reveals that many gas clouds form in the outskirts of the disc, while the central region has been evacuated by stellar feedback, giving rise to the wind. The temperature map illustrates nicely the hot gas in the wind, segregating from the cold gas in the ISM. Star formation still proceeds within dense clouds, but these are not long-lived anymore. This is why we do not see any massive star clusters in the stellar surface density map. Only a few managed to survive. This is one of the key qualitative features of our stellar feedback

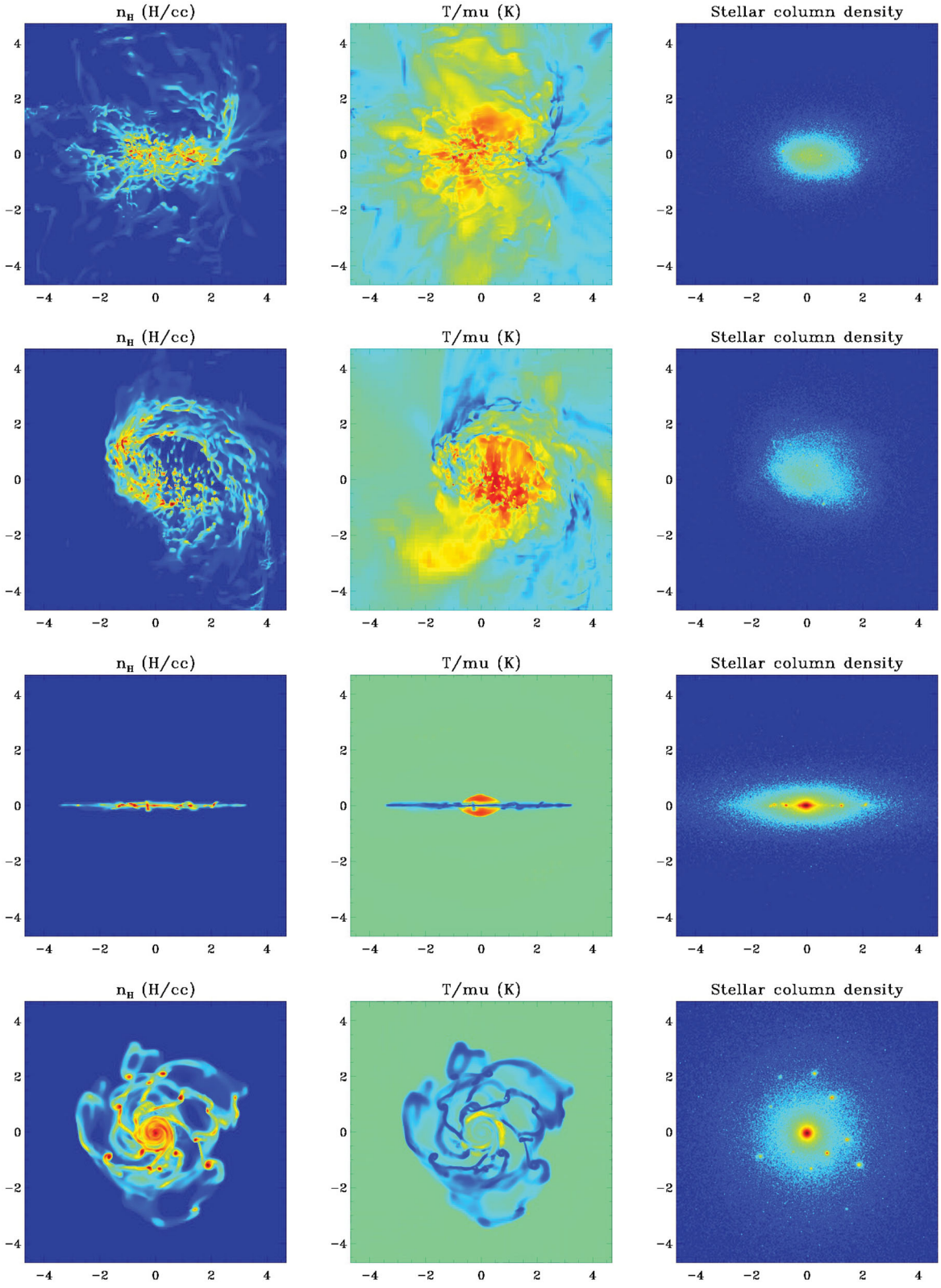

Figure 2. Maps of gas density (left, in logarithmic scale between 0.1 and 1000 H cm^{-3}), gas temperature (middle, in logarithmic scale between 300 and 10^6 K) and stellar column density (right, logarithmic scale in arbitrary units), seen face-on (lower plot) and side-on (upper plot), with (upper half) and without (lower half) feedback after 2 Gyr of evolution. The images are all 10 kpc across.

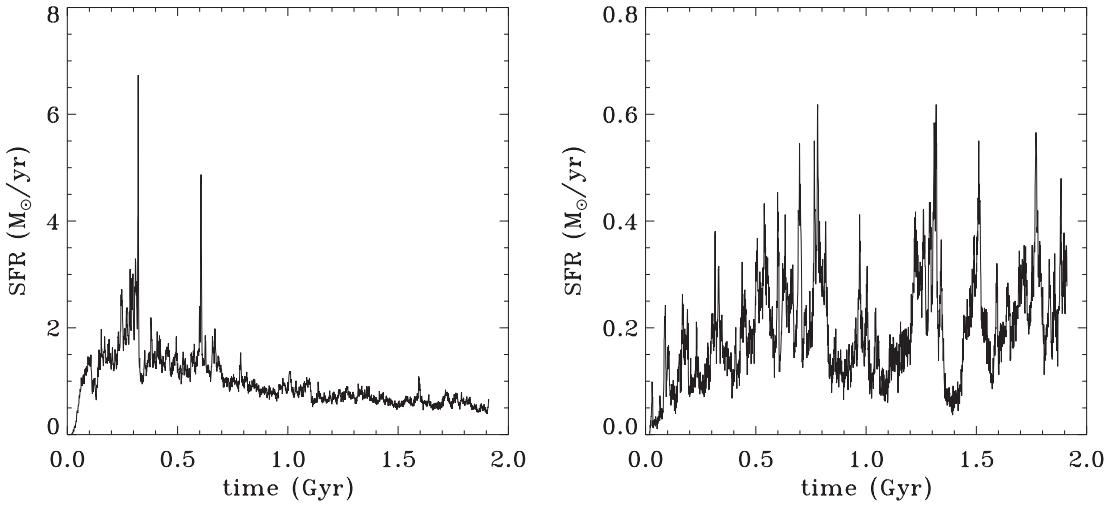

Figure 3. Star formation history in the runs without (left-hand plot) and with (right-hand plot) feedback.

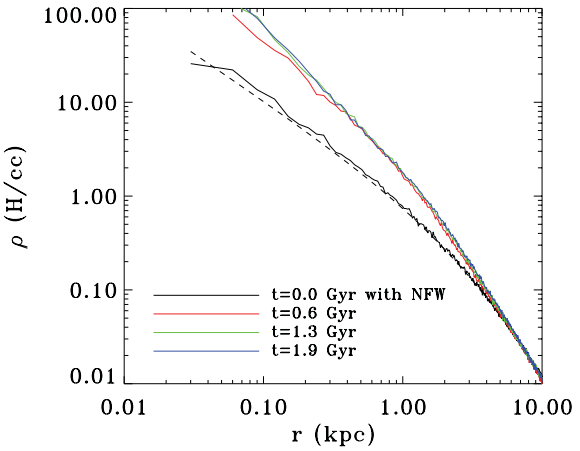

Figure 4. Evolution of the dark matter density profile over the 2 Gyr of evolution for the control run with cooling, star formation but no feedback. The dark matter halo has been strongly adiabatically contracted.

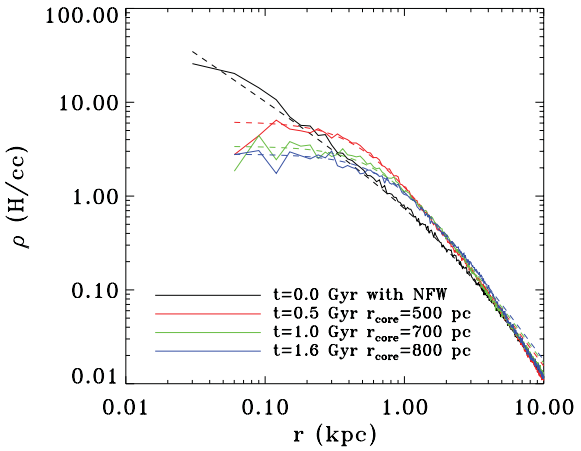

Figure 5. Evolution of the dark matter density profile over the 2 Gyr of evolution for the control run with cooling, star formation and stellar feedback. We see the formation of a large core. We also show for comparison the analytical fit (dashed line) based on a pseudo-isothermal profile (see the text for details).

implementation; gravitational instability and shock compression trigger the formation of star-forming clouds, which are then quickly disrupted by stellar feedback, recycling the unused gas into the ISM and giving rise to the galactic wind.

The SF rate plotted in Fig. 3 is one order of magnitude lower in average than the 'no feedback' case. It exhibits strong bursts followed by quiescent phases. When gas cools down and sinks towards the central region, SF rises sharply and triggers a starburst. Stellar feedback then removes the gas into the hot wind, leaving the central kpc almost devoid of gas. This explains the very low star formation episodes. Gas then rains back down from the corona and triggers a new SF episode. These cycles are clearly visible in the SF history. They are at the origin of strong potential fluctuations due to massive periodic gas outflows and inflows.

In Fig. 5, we plot the evolution of the dark matter density profile. As a technical side note, we would like to stress that these profiles have been computed using the highest dark matter density peak as centre, defined using the 'shrinking sphere' algorithm. This minimizes spurious features in the density profiles due to poor centring. We clearly see in the 'feedback' run that a large dark matter core develops. We tried to fit the resulting profile using a 'pseudo-isothermal' profile defined as

$$\rho \propto \frac{1}{1+(r/r_{\rm core})^2}. \qquad (9)$$

This analytical shape has traditionally been used in rotation curve fitting and has proven to work extremely well in nearby dwarf galaxies (Begeman, Broeils & Sanders 1991; Kuzio de Naray et al. 2006; Kuzio de Naray et al. 2008). As can be seen in Fig. 5, this is also true in our simulation, for which the pseudo-isothermal fit is remarkably good within the central 3–4 kpc. We have measured core radii ranging from 500 pc at early time (0.5 Gyr) to 800 pc at late time (1.6 Gyr). We do see a systematic increase of the core radius with time. We have also tried to fit our dark matter profile with other popular cored density distributions (Burkert 1995, for example) but with less success.

To quantify even more the time evolution of the dark matter distribution, we have fitted the density profile between 200 and 800 pc with a single power law (see Fig. 6). This is obviously a poor fit to our cored distribution, but this captures the essence of the dark

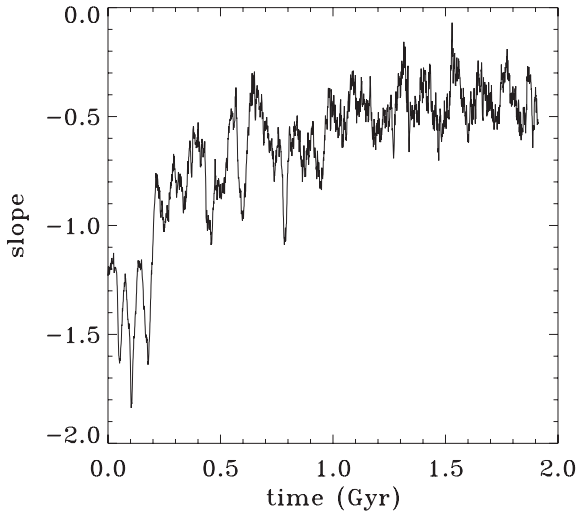

Figure 6. Time evolution of the slope of the dark matter density profile measured between 200 and 800 pc for the simulation with feedback.

matter flattening in the centre. At $t = 0$, we measure for the slope $\alpha = -1.2$, which is the average value of the NFW profile between the two chosen radii. At the beginning, gas cools down and adiabatic contraction of the halo can be measured as a decrease of the inner slope to $\alpha = -1.8$. But stellar feedback processes very quickly develop and trigger strong potential fluctuations, leading to a gradual flattening of the slope. We end up after 2 Gyr of evolution with a slope between $\alpha = -0.3$ and $\alpha = -0.5$, in excellent agreement with the measurement reported by PG12 in the context of a lower resolution cosmological simulation.

As proposed by PG12, this strongly suggests that the core formation mechanism is related to violent gas outflows triggered by a succession of starbursts. In order to validate this idea in our simulation, we have computed the time evolution of the enclosed gas mass within spheres of increasingly large radii, from 200 pc for the smallest to 1600 pc for the largest. The results are shown in Fig. 7 and illustrate that gas is repeatedly removed from the central region of the galaxy, giving rise to strong coherent potential fluctuations.

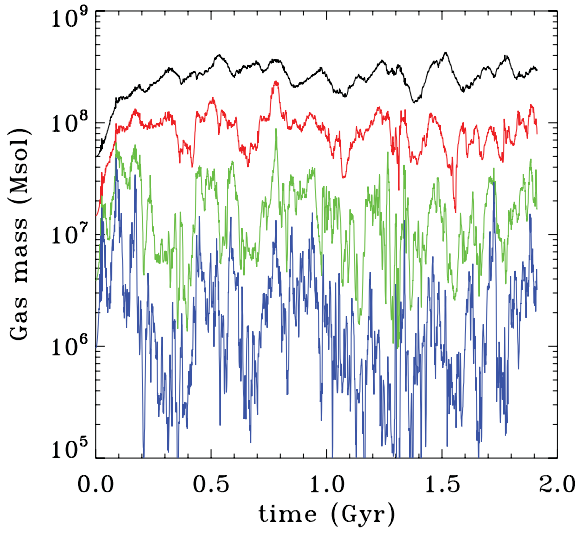

Figure 7. Time evolution of the total enclosed gas mass within spheres of radii 200 (blue), 400 (green), 800 (red) and 1600 (black) pc for the simulation with feedback.

As more gas cools down from the halo, the SF bursts become more violent and large mass fluctuations propagate to larger radii. This explains why we see a systematic increase in the dark matter core size as a function of time. At the end of the simulation, only scales up to ∼800 pc are affected by these strong fluctuations, corroborating nicely the measured core size of 800 pc.

While these results are qualitatively consistent with the analysis of PG12, there is a difference in the quantitative details. In our case, many potential fluctuations are not only established in a dynamical time (as in PG12) but are also erased before a full dynamical time has elapsed (unlike in PG12). The effect of these short-time transients is ignored by the PG12 toy model, since it starts by sampling the potential only once per dynamical time. Applying the PG12 algorithm directly, therefore, leads to incorrect predictions for our present simulation. We verified, however, that consistent predictions can be made by changing the sampling method to pick out, at each dynamical time step, the most extreme potential jump that occurred within the simulation. While this is a heuristic method, we believe it shows that the essential ingredient of impulsive potential changes is at play in our new simulations. It is in principle possible to extend the PG12 work to track phases of particles, thus giving a complete description of the impulsive changes which does not require the problematic quantization of time. However this approach would lose the attractive simplicity of the PG12 model and is certainly beyond the scope of the present investigation.

We should also emphasize that the core forms after only 0.5 Gyr in our reference feedback run, when only 10 per cent of the stars have formed. We have indeed measured a total stellar mass of $M_* \simeq 5 \times 10^7\,\mathrm{M}_\odot$ at that time. This means that the final total energy liberated in supernova explosions is not the limiting factor. This is in fact consistent with the estimates of energy required to form cores in Peñarrubia et al. (2012). The question of what limits star formation requires full cosmological runs to tackle further, since our 'monolithic collapse' models do not reflect the interplay between gas inflow, outflow and feedback that presumably regulate star formation as a function of redshift in the real universe.

5 OBSERVATIONAL GALAXY PROPERTIES

We have shown that cusp-core transformations are expected if there are strong (order unity) potential fluctuations on dynamical timescales. Such fluctuations are non-adiabatic, non-reversible, and heat both the dark matter and stars. We discuss here the observational consequences of such fluctuations; these can then be used to constrain or rule out the presence of such fluctuations in real systems.

5.1 The stellar distribution

Read & Gilmore (2005) found from their toy models that, when cusp-core transformations occur, the resulting surface brightness of the stars is well approximated by an exponential over many scale lengths, sometimes with a break radius at large radii and a core at small radii. This is exactly what we see in the present simulation; in Fig. 8, we have plotted the stellar surface density with and without feedback. In the latter case, we see a prominent bulge with high Sérsic index and a weak exponential disc extending up to 6 kpc, while in the feedback case, we see a smaller exponential disc, with no bulge in the centre and a clear signature of a stellar core within the central 500 pc. We have fitted this stellar distribution with a pure exponential disc with scale length $R_d = 1.1$ kpc (see Fig. 8). In our simulation without feedback, the stars form in a razor-thin, rotationally supported disc (see Fig. 9).

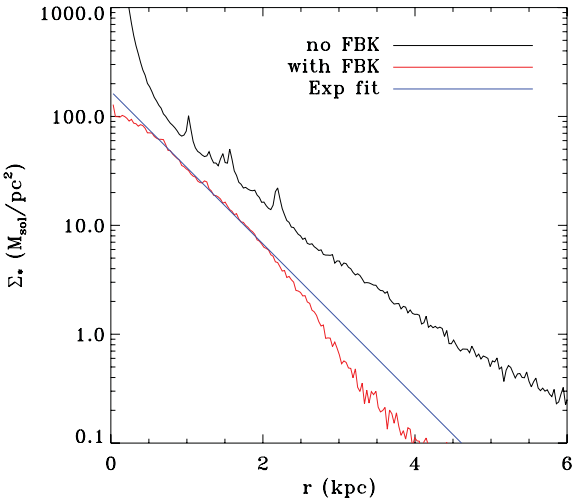

Figure 8. Stellar surface density of the final dwarf galaxy with (red line) and without (black line) feedback. In blue is shown the exponential fit of the stellar disc with feedback with scale length $R_d = 1.1$ kpc.

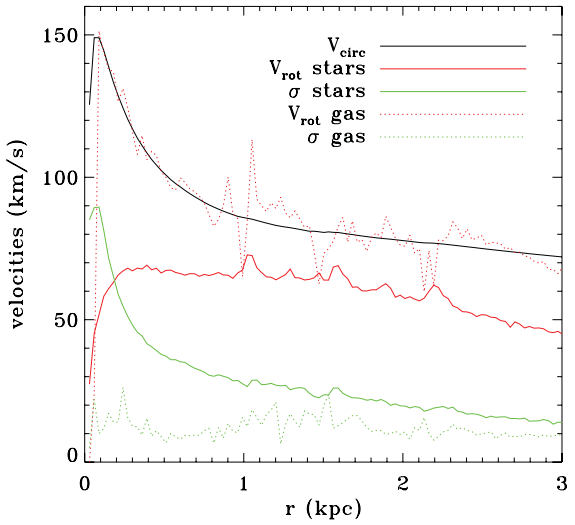

Figure 9. Kinematic analysis of our dwarf galaxy without feedback: circular velocities (black solid line), stellar tangential velocity (red solid line) and stellar tangential velocity dispersion (green solid line), compared to the gas tangential velocity (red dotted line) and gas tangential velocity dispersion (green dotted line).

Note that simulations of the formation and evolution of isolated dwarf galaxies generically end up with near-exponential surface brightness profiles, with rather thick gas and stellar discs (Springel & Hernquist 2003; Dubois & Teyssier 2008; Valcke et al. 2008). These simulations can be however divided into two main categories: quiescent feedback models, in which small-scale effects are captured by an effective equation of state, leading to a quiescent star formation history (SFH) where outflows are obtained through a quasi-stationary galactic wind (see e.g. Springel & Hernquist 2003; Dubois & Teyssier 2008), and bursty models, in which the SFH is not stationary and shows violent fluctuations (see e.g. Stinson et al. 2007; Valcke et al. 2008; Revaz et al. 2009). The first category of simulations give rise to moderately thick disc and very weak potential fluctuations. The stellar disc is still well defined with an aspect ratio close to $h/R \simeq 0.1$ (see fig. 11 in Springel & Hernquist 2003, for example). Therefore, we should not expect any dark matter core

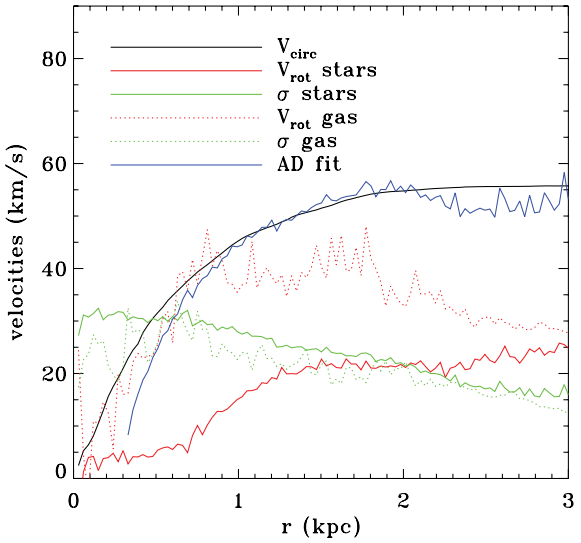

Figure 10. Kinematic analysis in the feedback case: circular velocities (black solid line), stellar tangential velocity (red solid line) and stellar tangential velocity dispersion (green solid line), compared to the gas tangential velocity (red dotted line) and gas tangential velocity dispersion (green dotted line). Also shown as the blue solid line is the predicted circular velocity curve based on the asymmetric drift (AD) approximation.

in this case. The second type of simulations, however, gives much thicker discs, in some case almost spheroidal galaxies. They show violently time-varying outflows, and they should lead to the formation of a dark matter core. Our present model, with strong stellar feedback, belongs to the second category; the resulting stellar distribution is oblate and quite hot, with $v/\sigma \simeq 1$ and a scale height to scale length ratio close to 0.5 (see Figs 2 and 10).

Unfortunately, it can be difficult to conclusively test the above expectations. Exponential surface brightness profiles can form through a variety of physical processes not related to violent potential fluctuations (e.g. Lin & Pringle 1987). Similarly, hot stellar distributions with $v/\sigma \sim 1$ need not be a smoking gun for cusp/core transformations. Galactic mergers (e.g. Searle & Zinn 1978; Read, Pontzen & Viel 2006b) and collisionless heating from a strong tidal field (e.g. Mayer et al. 2001; Lokas, Kazantzidis & Mayer 2011) both lead to stellar distributions with low v/σ.

We can avoid all of the above complications, however, if we focus on *isolated* low-mass dwarf galaxies. The best-studied system to date is WLM. Despite being extremely tidally isolated, WLM does indeed have a hot, oblate spheroidal, stellar distribution (with $v/\sigma \simeq 1$ and $h/R_d \simeq 0.5$) that is reasonably approximated by an exponential surface brightness fall-off (Leaman et al. 2012). Note that in this case too, a flattening on the stellar surface density profile is seen in the centre, reminiscent of a stellar core.[1] Leaman et al. (2012) point out that it may be difficult to understand why the stellar distribution in WLM is so hot without recourse to strong and bursty stellar feedback. We can confirm that view here. In our model of an isolated dwarf galaxy, only the simulation with very strong feedback managed to form a hot thick-disc-like stellar distribution. This same simulation found a significant cusp-core transformation in the underlying dark matter distribution. In order to push the comparison with WLM even further, we have analysed the kinematic properties

[1] PG12 pointed out the heating processes applying to the DM should also apply to the stars.

of our dwarf galaxy. These are shown in Fig. 10. One can see immediately that the stellar rotation curve is slowly rising, while the stellar velocity dispersion is slowly declining. Both curves intersect at around 2 kpc, at a value close to 20 km s^{-1}. These features are in striking agreement with WLM data as exposed in Leaman et al. (2012). The gas kinematic properties are also very similar, as shown in Fig. 10. Using our kinematic analysis, we are in a good position to test one important method to derive the total mass profile in dwarf galaxies from their kinematic properties, namely the asymmetric drift (AD) model. This method, based on the Jeans equation, follows a few reasonable simplifying assumptions to derive the relation between the circular velocity and the velocity moments. Following Hinz, Rix & Bernstein (2001) and Leaman et al. (2012), we used $v_{\rm circ}^2 = v_\theta^2 + \sigma_\theta^2\,(2r/R_d - 1)$ with $R_d \simeq 1.1$ kpc, as measured in our simulation. We see in Fig. 10 that AD is overall a good approximation to recover the underlying mass profile, except perhaps in the very centre where it is underestimated. The total mass inferred from this analysis by Leaman et al. (2012) for WLM, $M_{\rm tot} \simeq 2 \times 10^{10}\,{\rm M}_\odot$ is therefore accurate, and again very close to our simulated halo mass.

Although our spatial and kinematic properties are in striking agreement with the relatively isolated dwarf WLM, the total stellar mass that we obtained in our simulation is too large by one order of magnitude. We have plotted in Fig. 11 the cumulative stellar mass profile in spherical shells. One sees clearly that without feedback, almost all baryons are converted into stars after 1 Gyr, since we get $M_* \simeq 10^9\,{\rm M}_\odot$. With our strong stellar feedback model, we managed to reduce this number by one order of magnitude, down to $M_* \simeq 10^8\,{\rm M}_\odot$. This is quite an achievement, but it falls short by one order of magnitude to explain the stellar mass observed in WLM, which has been measured by Jackson et al. (2007) to be $M_* \simeq 1.1 \times 10^7\,{\rm M}_\odot$. We are therefore overproducing stars to a level comparable to most current galaxy formation simulations (Piontek & Steinmetz 2009; Governato et al. 2010; Agertz et al. 2011), when compared to individual galaxies or to an ensemble of galaxies using the abundance matching technique (Guo et al. 2010; Moster et al. 2010), although recently Munshi et al. (2012) argue differently. Although solving this issue is beyond the scope of this paper, we have a conceptually simple way to solve this problem, by lowering the star formation efficiency parameter ϵ_* by one order of magnitude, and in the same time, increasing the mass fraction of massive star going supernovae by also one order of magnitude. The first idea could be justified by the low metallicity we find in dwarf galaxies, leading to a inefficient regime of star formation, for which dust shielding is less efficient at promoting H_2 molecule formation (Krumholz & Dekel 2011). The second idea could be justified by recent observations of low metallicity star clusters in the Galaxy, which are consistent with a top-heavy IMF (Marks et al. 2012). Using these two non-standard but plausible ingredients, we will straightforwardly obtain the same energy input from supernovae, and therefore the same hydrodynamical model, with however 10 times less *long-lived* star formed. A different model based on early radiative stellar feedback has been recently proposed by Brook et al. (2012) that could solve this very same issue, although the quantitative effect would not be as straightforward as the one proposed here.

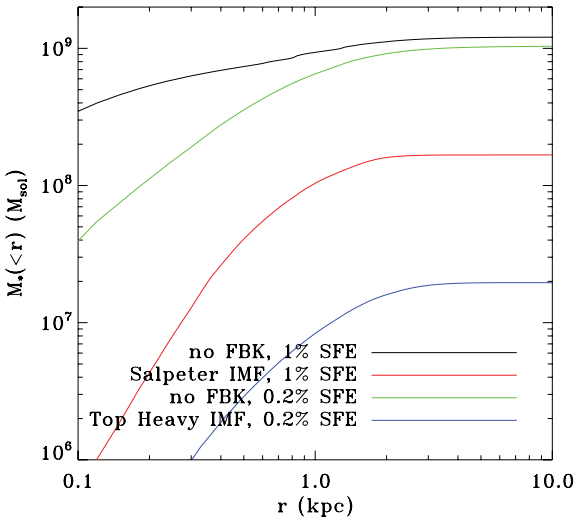

Figure 11. Cumulative stellar mass profile as a function of spherical radius for the fiducial star formation efficiency (1 per cent) without (black line) and with (red line) stellar feedback at $t \simeq 1$ Gyr. Also shown are the stellar mass profiles with a very low star formation efficiency (0.2 per cent) and a top heavy IMF, without (green line) and with (blue line) stellar feedback. Only the latter model can match the observed stellar mass in the dwarf galaxy WLM.

Since complex non-linear hydrodynamical processes are at play, it is not obvious that lowering ϵ_* (while increasing the feedback energy per stellar mass formed) will result in decreasing the total stellar mass formed. We therefore run two additional simulations with $\epsilon_* = 0.2$ per cent and a top-heavy IMF so that 50 per cent of the mass of a given stellar population (or star particle) will be in massive stars going supernovae. The first simulation was run without stellar feedback (only metal enrichment) and the second simulation was run with our new stellar feedback scheme and a top-heavy IMF. We have plotted in Fig. 11 the cumulative stellar mass profiles of these two additional runs. Interestingly, although we have decreased by a factor of 5 the SFE, the run without feedback gives also rise to the formation of $M_* \simeq 10^9\,{\rm M}_\odot$ of stars, like in the fiducial case. This means that, without stellar feedback, the gaseous disc always manages to cool and contract enough to reach high gas densities and transform most of its baryons into stars. With stellar feedback, however, we form only $M_* \simeq 2 \times 10^7\,{\rm M}_\odot$ of stars after 1 Gyr, in much better agreement with the observed stellar mass in WLM. We have also checked (not shown here) that, in this last simulation, all of the galaxy properties discussed above are also recovered, namely a large dark matter core, thick stellar and gaseous discs and a bursty SF history, with large amount of gas moving in and out of the central kpc of the galaxy. This last model gives very encouraging results, but requires a significantly top-heavy IMF together with a very low star formation efficiency. We would like also to stress again (see Section 4) that star formation might be also regulated or even stopped after only 0.5 Gyr of evolution, due to the effect of a more realistic cosmological accretion history, which is not captured here in this idealized set-up.

5.2 Star formation histories

A second key observational prediction of cusp-core transformations is the SFH. In the category of feedback models where cusp-core transformations are expected (Stinson et al. 2007; Valcke et al. 2008; Revaz et al. 2009; Cloet-Osselaer et al. 2012, and this paper), the SFH is extremely bursty with peak to trough variations of 10 and a duty cycle of roughly one dynamical time. Although our *average* star formation rate of 0.02 to 0.2 ${\rm M}_\odot\,{\rm yr}^{-1}$ for a total gas mass of $10^9\,{\rm M}_\odot$ is consistent with observations of blue compact dwarf galaxies in the local universe (Hopkins et al. 2002), the bursty nature of its time evolution needs to be tested observationally. There are

two possibilities: (i) measure the SFH for individual systems and (ii) estimate the *variance* in the star formation statistically for a large population of like-galaxies. The former is cleaner, but requires very high time resolution in the derived SFH; the latter has potentially high time resolution but relies on assumptions about the equivalence of large populations of galaxies. We discuss each in turn, next.

5.2.1 *Individual star formation histories*

The best SFHs come from the most nearby systems. These have resolved colour magnitude diagrams (CMDs) that reach the oldest main sequence turn-offs, which is vital for correctly recovering the intermediate age stars (e.g. Noël et al. 2009). More distant systems have SFHs derived via spectral energy distribution fitting of the unresolved stars that is degenerate and less accurate than CMD fitting (e.g. Zhang et al. 2012).

The best-studied system to date is the nearby dwarf spheroidal galaxy Sculptor that orbits the Milky Way (e.g. Mateo 1998; Lux, Read & Lake 2010). Unfortunately, even for excellent data, CMD fitting has a temporal resolution poorer than ∼1 Gyr (Dolphin 2002), where the errors come from a mix of photometric uncertainty, spread in distance modulus and errors in the stellar population evolution libraries (Dolphin 2012). de Boer et al. (2012) have recently attempted to improve this situation by simultaneously fitting the CMD and spectroscopic metallicities of red giant branch stars. They explicitly consider how well their methodology could recover a bursty SFH. Using simulated data, they show that their method would recover a smooth continuous SFH (as observed for Sculptor) from an input bursty history. Thus, the very best data remain inconclusive. It is interesting to note, however, that the very latest dynamical models for Sculptor appear to favour a cored rather than cusped mass distribution (Battaglia et al. 2008; Walker & Peñarrubia 2011; Amorisco & Evans 2012). This motivates a continued effort to attempt to confirm or deny a highly bursty SFH for Sculptor.

5.2.2 *The star formation history of a population of dwarf galaxies*

An alternative approach to studying individual galaxies is to study a population statistically. If we assume that all dwarf galaxies of a given mass and type are statistically equivalent, then we can treat these as individual sample points along the SFH. If the SFH is smooth and continuous, then the variance in the measured SFH for the population will be small; if, however, it is bursty, then the variance will be larger. Weisz et al. (2012) have recently used this idea to test a simple bursty SFH against a population of 185 galaxies from the *Spitzer* Local Volume Legacy survey. They find that their more massive galaxies ($M_* \geq 10^7\,\mathrm{M}_\odot$) are better fit (on average) by a smooth and continuous SFH, while the lower mass systems ($M_* \leq 10^7\,\mathrm{M}_\odot$) favour a bursty SFH with bursts of ∼10s of Myr, inter-burst periods of ∼250 Myr and peak to trough burst amplitude ratios of ∼30. These numbers are in total agreement with the SFH we obtained for our model with a cusp-core transformation (see Fig. 3). WLM is again interesting here. It has a stellar mass of $1.1 \times 10^7\,\mathrm{M}_\odot$ and a dynamical mass of $\sim 10^{10}\,\mathrm{M}_\odot$ (Leaman et al. 2012). As we have shown, it is comparable to our simulated halo, and statistically in the stellar mass range where bursty star formation in dwarf galaxies is observationally favoured.

It seems that all of the currently available data favour a bursty SFH for dwarf galaxies with stellar mass $\leq 10^7\,\mathrm{M}_\odot$ and dynamical mass $\leq 10^{10}\,\mathrm{M}_\odot$. As we have shown here, such a bursty SFH will naturally heat the stars producing a hot stellar distribution even in isolated systems, consistent with recent observations of the isolated dwarf galaxy WLM. It also drives cusp-core transformations in the dark matter that can explain the now long-standing cusp-core problem (Flores & Primack 1994; Moore 1994).

6 DISCUSSION

In this paper, we have simulated an isolated dwarf galaxy using the now traditional set-up of the cooling halo. Using a new implementation of stellar feedback within the RAMSES code, we have modelled the formation of a dwarf galaxy of $10^{10}\,\mathrm{M}_\odot$ halo mass, whose evolution has been shown to be strongly dominated by feedback processes. We have observed the formation of a 800 pc dark matter core, the size of which corresponds roughly to 40 resolution elements. We have analysed in details the stellar distribution and kinematics of our model galaxy, observable properties that compare successfully to the local isolated dwarf WLM. In our fiducial model, the total stellar mass is too large by one order of magnitude, suggesting that we need to lower the long-lived star formation efficiency, while keeping the same overall feedback efficiency to match all constraints. We have shown that this might be indeed achieved, if one uses a very low value for the Schmidt law parameter $\epsilon_* \simeq 0.2$ per cent, together with a top-heavy IMF.

Our simulation with feedback and AMR clearly confirms previous works performed with various SPH codes, both for isolated haloes and in a cosmological context, at a somewhat lower resolution than the one used here. The temporal variations and systematic evolution of the inner slope of the dark matter profile correlate nicely with bursts seen in the SF history of our dwarf galaxy. We noted that there are several observational diagnostics which point to the cusp-flattening process driven by bursty star formation. The most obvious place to look is in star formation histories. Unfortunately for individual cases, it is unlikely to be possible to achieve sufficient time resolution (e.g. de Boer et al. 2012; Dolphin 2012). On the other hand, statistical studies of populations encouragingly point to bursts of exactly the right nature for cusp-flattening, and in agreement with our work, especially at low masses (Weisz et al. 2012). There may be less direct evidence of a cusp-flattening process in the final kinematics of the stars. Since stars behave as collisionless particles, like dark matter, they should be heated by the irreversible process proposed by Read & Gilmore (2005), Mashchenko et al. (2006) and Pontzen & Governato (2012). Indeed when cusp-flattening occurs, we also obtain hotter, more oblate stellar distributions with $v/\sigma \simeq 1$. More directly related to the proposed mechanism, we also obtain a core in the stellar distribution. Promisingly, this also agrees well with the recent observations of the isolated dwarf galaxy WLM (Leaman et al. 2012).

Although these observations tend to favour bursty SF histories as a plausible origin to cusp-core transformations, we would like to stress that this is only a necessary condition for these to occur, not a sufficient one; other physical mechanisms could be at play to explain cusp-core transformations, not related to baryonic processes, but, for example, to warm or self-interacting dark matter particles.

ACKNOWLEDGMENTS

We thank our anonymous referee for helpful suggestions that greatly improved the quality of the paper. We thank Pascale Jablonka for interesting discussions on the SFH of dwarf galaxies. JR would like to acknowledge support from SNF grant PP00P2_128540/1. The simulations presented here were performed on the COAST cluster at IRFU, CEA Saclay.

REFERENCES

Agertz O., Teyssier R., Moore B., 2009, MNRAS, 397, L64
Agertz O., Teyssier R., Moore B., 2011, MNRAS, 410, 1391
Agertz O. et al., 2007, MNRAS, 380, 963
Amorisco N. C., Evans N. W., 2012, MNRAS, 419, 184
Battaglia G., Helmi A., Tolstoy E., Irwin M., Hill V., Jablonka P., 2008, ApJ, 681, L13
Begeman K. G., Broeils A. H., Sanders R. H., 1991, MNRAS, 249, 523
Bournaud F. et al., 2011, ApJ, 730, 4
Brook C. B., Stinson G., Gibson B. K., Wadsley J., Quinn T., 2012, MNRAS, 424, 1275
Bullock J. S., Dekel A., Kolatt T. S., Kravtsov A. V., Klypin A. A., Porciani C., Primack J. R., 2001, ApJ, 555, 240
Burkert A., 1995, ApJ, 447, L25
Ceverino D., Klypin A., 2009, ApJ, 695, 292
Cloet-Osselaer A., De Rijcke S., Schroyen J., Dury V., 2012, MNRAS, 423, 735
de Blok W. J. G., Bosma A., 2002, A&A, 385, 816
de Blok W. J. G., McGaugh S. S., 1997, MNRAS, 290, 533
de Blok W. J. G., McGaugh S. S., Bosma A., Rubin V. C., 2001, ApJ, 552, L23
de Boer T. J. L. et al., 2012, A&A, 539, 103
Dekel A., Silk J., 1986, ApJ, 303, 39
Dolphin A. E., 2002, MNRAS, 332, 91
Dolphin A. E., 2012, ApJ, 751, 60
Dubois Y., Teyssier R., 2008, A&A, 477, 79
El-Zant A., Shlosman I., Hoffman Y., 2001, ApJ, 560, 636
Ellison D. C., Decourchelle A., Ballet J., 2004, A&A, 413, 189
Enßlin T. A., Pfrommer C., Springel V., Jubelgas M., 2007, A&A, 473, 41
Ferrand G., Decourchelle A., Ballet J., Teyssier R., Fraschetti F., 2010, A&A, 509, L10
Flores R. A., Primack J. R., 1994, ApJ, 427, L1
Fromang S., Hennebelle P., Teyssier R., 2006, A&A, 457, 371
Goerdt T., Moore B., Read J. I., Stadel J., 2010, ApJ, 725, 1707
Governato F. et al., 2010, Nat, 463, 203
Guo Q., White S., Li C., Boylan-Kolchin M., 2010, MNRAS, 404, 1111
Hanasz M., Otmianowska-Mazur K., Kowal G., Lesch H., 2006, Astron. Nachr., 327, 469
Hinz J. L., Rix H.-W., Bernstein G. M., 2001, AJ, 121, 683
Hopkins A. M., Schulte-Ladbeck R. E., Drozdovsky I. O., 2002, AJ, 124, 862
Hopkins P. F., Quataert E., Murray N., 2012, MNRAS, 421, 3488
Jackson D. C., Skillman E. D., Gehrz R. D., Polomski E., Woodward C. E., 2007, ApJ, 656, 818
Jubelgas M., Springel V., Enßlin T., Pfrommer C., 2008, A&A, 481, 33
Katz N., Weinberg D. H., Hernquist L., 1996, ApJS, 105, 19
Kaufmann T., Mayer L., Wadsley J., Stadel J., Moore B., 2007, MNRAS, 375, 53
Kazantzidis S., Magorrian J., Moore B., 2004, ApJ, 601, 37
Krumholz M. R., Dekel A., 2012, ApJ, 753, 16
Krumholz M. R., Tan J. C., 2007, ApJ, 654, 304
Kuzio de Naray R., McGaugh S. S., de Blok W. J. G., Bosma A., 2006, ApJS, 165, 461
Kuzio de Naray R., McGaugh S. S., de Blok W. J. G., 2008, ApJ, 676, 920
Kuzio de Naray R., Martinez G. D., Bullock J. S., Kaplinghat M., 2010, ApJ, 710, L161
Leaman R. et al., 2012, ApJ, 750, 33
Lin D. N. C., Pringle J. E., 1987, ApJ, 320, L87
Lokas E. L., Kazantzidis S., Mayer L., 2011, ApJ, 739, 46
Lux H., Read J. I., Lake G., 2010, MNRAS, 406, 2312
Macciò A. V., Paduroiu S., Anderhalden D., Schneider A., Moore B., 2012, MNRAS, 424, 1105
Marks M., Kroupa P., Dabringhausen J., Pawlowski M. S., 2012, MNRAS, 422, 2246
Martizzi D., Teyssier R., Moore B., Wentz T., 2012, MNRAS, 422, 3081
Mashchenko S., Couchman H. M. P., Wadsley J., 2006, Nat, 442, 539
Mashchenko S., Wadsley J., Couchman H. M. P., 2008, Sci, 319, 174
Mateo M. L., 1998, ARA& A, 36, 435
Mayer L., Governato F., Colpi M., Moore B., Quinn T., Wadsley J., Stadel J., Lake G., 2001, ApJ, 559, 754
Moore B., 1994, Nat, 370, 629
Moster B. P., Somerville R. S., Maulbetsch C., van den Bosch F. C., Macciò A. V., Naab T., Oser L., 2010, ApJ, 710, 903
Munshi F. et al., 2012, preprint (arXiv:1209.1389)
Murray N., Quataert E., Thompson T. A., 2010, ApJ, 709, 191
Navarro J. F., Eke V. R., Frenk C. S., 1996, MNRAS, 283, L72
Navarro J. F., Frenk C. S., White S. D. M., 1997, ApJ, 490, 493
Noël N. E. D., Aparicio A., Gallart C., Hidalgo S. L., Costa E., Méndez R. A., 2009, ApJ, 705, 1260
Peñarrubia J., Pontzen A., Walker M. G., Koposov S. E., 2012, ApJ, 759, 42
Piontek F., Steinmetz M., 2011, MNRAS, 410, 2625
Pontzen A., Governato F., 2012, MNRAS, 421, 3464 (PG12)
Read J. I., Gilmore G., 2005, MNRAS, 356, 107
Read J. I., Hayfield T., 2012, MNRAS, 422, 3037
Read J. I., Wilkinson M. I., Evans N. W., Gilmore G., Kleyna J. T., 2006a, MNRAS, 367, 387
Read J. I., Pontzen A. P., Viel M., 2006b, MNRAS, 371, 885
Read J. I., Hayfield T., Agertz O., 2010, MNRAS, 405, 1513
Revaz Y. et al., 2009, A&A, 501, 189
Rocha M., Peter A. H. G., Bullock J. S., Kaplinghat M., Garrison-Kimmel S., Onorbe J., Moustakas L. A., 2012, preprint (arXiv:1208.3025)
Rosen A., Bregman J. N., 1995, ApJ, 440, 634
Scannapieco E., Brüggen M., 2010, MNRAS, 405, 1634
Scannapieco C., Wadepuhl M., Parry O. H., Navarro J. F., Jenkins A., Springel V., Teyssier R., 2012, MNRAS, 423, 1726
Schmidt M., 1959, ApJ, 129, 243
Schroyen J., De Rijcke S., Valcke S., Cloet-Osselaer A., Dejonghe H., 2011, MNRAS, 416, 601
Searle L., Zinn R., 1978, ApJ, 225, 357
Spergel D. N., Steinhardt P. J., 2000, Phys. Rev. Lett., 84, 3760
Springel V., 2005, MNRAS, 364, 1105
Springel V., Hernquist L., 2003, MNRAS, 339, 289
Stinson G., Seth A., Katz N., Wadsley J., Governato F., Quinn T., 2006, MNRAS, 373, 1074
Stinson G. S., Dalcanton J. J., Quinn T., Kaufmann T., Wadsley J., 2007, ApJ, 667, 170
Sutherland R. S., Dopita M. A., 1993, ApJS, 88, 253
Teyssier R., 2002, A&A, 385, 337
Teyssier R., Fromang S., Dormy E., 2006, J. Comput. Phys., 218, 44
Teyssier R., Chapon D., Bournaud F., 2010, ApJ, 720, L149
Truelove J. K., Klein R. I., McKee C. F., Holliman J. H. I., Howell L. H., Greenough J. A., 1997, ApJ, 489, L179
Uhlig M., Pfrommer C., Sharma M., Nath B. B., Enßlin T. A., Springel V., 2012, MNRAS, 423, 2374
Valcke S., De Rijcke S., Dejonghe H., 2008, MNRAS, 389, 1111
Villaescusa-Navarro F., Dalal N., 2011, J. Cosmol. Astropart. Phys., JCAP03(2011)024
Wadsley J. W., Stadel J., Quinn T., 2004, New Astron., 9, 137
Wadsley J. W., Veeravalli G., Couchman H. M. P., 2008, MNRAS, 387, 427
Walker M. G., Peñarrubia J., 2011, ApJ, 742, 20
Weisz D. R. et al., 2012, ApJ, 744, 44
Williams J. P., McKee C. F., 1997, ApJ, 476, 166
Zhang H.-X., Hunter D. A., Elmegreen B. G., Gao Y., Schruba A., 2012, AJ, 143, 47

This paper has been typeset from a TEX/LATEX file prepared by the author.